Journal of Organometallic Chemistry 937 (2021) 121704

Contents lists available at ScienceDirect

Journal of Organometallic Chemistry

journal homepage: www.elsevier.com/locate/jorganchem

Mild intramolecular P–C(sp^3) bond cleavage in bridging diphosphine complexes of Ru^{II} Rh^{III} and Ir^{III} ☆

Peter De'Ath, Mark R.J. Elsegood, Christopher A.G. Halliwell, Martin B. Smith*

Department of Chemistry, Loughborough University, Loughborough, Leics, LE11 3TU, UK

ARTICLE INFO

Article history:
Received 30 November 2020
Revised 4 January 2021
Accepted 10 January 2021
Available online 16 January 2021

Keywords:
Carboxylic acids
P ligands
Late-transition metals
X-ray crystallography
P–C bond cleavage

ABSTRACT

Three new carboxylic acid functionalised diphosphines, $R_2PCH_2N(Ar)CH_2PR_2$ [^{Cy}**L$_1$** R = Cy, Ar = (1-CO_2H)(3-OMe)C_6H_3, ^{Cy}**L$_2$** R = Cy, Ar = (1-CO_2H)(3-OH)C_6H_3 and ^{Ph}**L$_3$** R = Ph, Ar = (1-CO_2H)(5-OMe)C_6H_3] have been prepared from condensation of R_2PCH_2OH and the appropriate aromatic amine in MeOH, and isolated as colourless solids (for ^{Cy}**L$_1$**, ^{Cy}**L$_2$**) in good yield. Reaction of ^{Cy}**L$_1$**, ^{Cy}**L$_2$**, or ^{Ph}**L$_3$**, along with the previously reported diphosphines ^{Ph}**L$_1$**, ^{Ph}**L$_2$**, and ^{Ph}**L$_4$**, and $[RuCl(\mu\text{-}Cl)(\eta^6\text{-}Me_2CHC_6H_4Me)]_2$ in CH_2Cl_2 affords the P/P-bridging dinuclear ruthenium(II) complexes $\{RuCl_2(\eta^6\text{-}Me_2CHC_6H_4Me)\}_2(\mu\text{-}^{Cy}L_1\text{–}^{Ph}L_4)$ **1a–f** as red/orange solids. Careful monitoring by $^{31}P\{^1H\}$ NMR spectroscopy of $CDCl_3$ solutions of **1a–e** revealed remarkably clean P–C$_{sp3}$ bond cleavage to give Ru^{II} mononuclear species **2a–e** and the known secondary phosphine complexes $RuCl_2(\eta^6\text{-}Me_2CHC_6H_4Me)(PCy_2H)$ **3** and $RuCl_2(\eta^6\text{-}Me_2CHC_6H_4Me)(PPh_2H)$ **4**. Furthermore, facile P–C$_{sp}{}^3$ bond cleavage of ^{Ph}**L$_1$** can be observed using the chloro-bridged dimers $[IrCl(\mu\text{-}Cl)(\eta^5\text{-}C_5Me_5)]_2$ or $[RhCl(\mu\text{-}Cl)(\eta^5\text{-}C_5Me_5)]_2$ instead. Deuterium labelling of ^{Cy}**L$_1$**, ^{Cy}**L$_1$**, ^{Ph}**L$_1$**, and ^{Ph}**L$_2$** enabled the assignment of the methylene protons to be confirmed from ^{1}H NMR spectroscopy. All new compounds have been characterised using a range of spectroscopic and analytical techniques. Single crystal X-ray structures have been determined for ^{Cy}**L$_1$**, **1d**·3OEt_2, **1f**·2$CDCl_3$·OEt_2, **2b, 2c, 2d**·$CDCl_3$, **2e**·0.5OEt_2 and **6b**·1.5$CDCl_3$. The free phenolic group in ^{Cy}**L$_1$**, **1d**·3OEt_2, **1f**·2$CDCl_3$·OEt_2, **2b** and **2d**·$CDCl_3$ participates in intra- or intermolecular O–H···O hydrogen bonding.

1. Introduction

Tertiary phosphines are routinely used in many disciplines of inorganic, organic, material, and biological sciences. Their versatility stems from easy manipulation of the chemical structure of these important ligands, which are often regarded as chemically robust with respect to decomposition [1,2]. Common degradation pathways to phosphine ligands include oxidation and P–C$_{aryl}$ [3] or P–C$_{alkyl}$ [4] bond cleavage reactions. Chelating diphosphines are widely used in transition metal chemistry and can also be susceptible to thermal/chemical induced P–C bond activation at one (or more) metal centres [5]. We [6], and others [7,8], have been interested for several years in the chemistry of chelating (aminomethyl)phosphines such as $(R_2PCH_2)_2N(R')$ (R = Ph typically, R' = various substituents), a close relative of the widely used ligand $(Ph_2PCH_2)_2CH_2$ (**dppp**, Chart 1). Their amenability, through simple condensation reactions, enables rapid functionalisation of the P–C–N–C–P framework at either or both Group 15 donor atoms. To the best of our knowledge, only one example of P–C bond cleavage at a coordinated P–C–N–C–P ditertiary phosphine has been documented [9], whereas Starosta and co-workers [10] have reported P–C cleavage of a tertiary aminomethylphosphine affording an unusual secondary phosphine coordination complex.

We report here a facile, internal acid-promoted, P–C bond cleavage within the coordination sphere of a diruthenium centre and clean formation of two monomeric species bearing either a bound secondary phosphine [10] or lactone-functionalised P-monodentate ligand. Bullock *et al* [11] have extensively used earth-abundant metal catalysts based on P–C–N–C–P ligand scaffolds for hydrogen oxidation or production. A crucial step in this process involves protonation at the pendant nitrogen atom, and this is influenced by the six-membered chelate ring conformation [11]. The structures of all new compounds reported in this work, including dinuclear Ru^{II} compounds supported by a bridging P–C–N–C–N ligand, have been verified by a combination of spectroscopic and X-ray crystallographic characterisation techniques.

☆ Electronic supplementary information (ESI) available. CCDC 2022153-60. For ESI and crystallographic data in CIF or other electronic format see DOI.

* Corresponding author.
E-mail address: m.b.smith@lboro.ac.uk (M.B. Smith).

https://doi.org/10.1016/j.jorganchem.2021.121704
0022-328X/

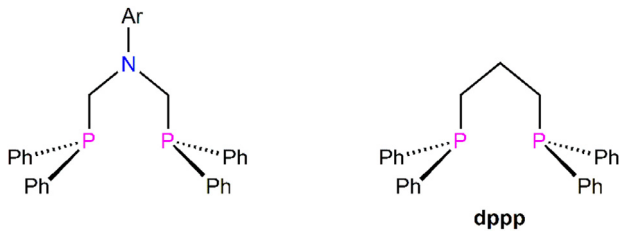

Chart 1. PCNCP structural motif and relationship to dppp.

2. Experimental

2.1. Materials

The synthesis of ligands $^{Ph}\mathbf{L_1}$, $^{Ph}\mathbf{L_2}$, and $^{Ph}\mathbf{L_4}$ has been reported previously by us [6e,6f] whilst ligands $^{Cy}\mathbf{L_1}$, $^{Cy}\mathbf{L_2}$, and $^{Ph}\mathbf{L_3}$ were prepared using standard Schlenk-line techniques under an inert nitrogen atmosphere. Ph_2PCH_2OH was prepared [12] according to a known procedure and Cy_2PCH_2OH, Ph_2PCD_2OH, and Cy_2PCD_2OH were likewise prepared similarly, from either Ph_2PH or Cy_2PH and $(CD_2O)_n$. All coordination reactions were carried out in air, using reagent grade quality solvents. The compounds $[RuCl(\mu\text{-}Cl)(\eta^6\text{-}Me_2CHC_6H_4Me)]_2$ [13], $[RhCl(\mu\text{-}Cl)(\eta^5\text{-}C_5Me_5)]_2$ [14] and $[IrCl(\mu\text{-}Cl)(\eta^5\text{-}C_5Me_5)]_2$ [14] were all prepared according to known procedures. All other chemicals were obtained from commercial sources and used directly without further purification.

2.2. Instrumentation

Infrared spectra were recorded as KBr pellets on a Perkin-Elmer Spectrum 100S (4000–250 cm^{-1} range) Fourier-Transform spectrometer. ^1H NMR spectra (400 or 500 MHz) were recorded on a Jeol-ECS-400 FT or Jeol-ECZ-R-500 spectrometer with chemical shifts (δ) in ppm to high frequency of $Si(CH_3)_4$ and coupling constants (J) in Hz. $^{31}P\{^1H\}$ NMR (162 or 202 MHz) spectra were recorded on a Jeol-ECS-400 FT or Jeol-ECZ-R-500 spectrometer with chemical shifts (δ) in ppm to high frequency of 85% H_3PO_4. NMR spectra were measured in $CDCl_3$, $(CD_3)_2SO$ or CD_3OD at 298 K. Elemental analyses (Perkin-Elmer 2400 CHN or Exeter Analytical, Inc. CE-440 Elemental Analyzers) were performed by the Loughborough University Analytical Service within the Department of Chemistry. Single crystal X-ray crystallography was carried out by the UK National Crystallographic Service at the University of Southampton or locally by ourselves at Loughborough University.

2.3. Syntheses

2.3.1. Synthesis of $Cy_2PCH_2N(Ar)CH_2PCy_2$ [Ar = $C_6H_3(1\text{-}CO_2H)(3\text{-}OMe)$] $^{Cy}L_1$

2-amino-3-methoxybenzoic acid (0.345 g, 2.07 mmol) and Cy_2PCH_2OH (0.936 g, 4.14 mmol) were dissolved in CH_3OH (30 mL) and stirred under reflux for 24 h. The resulting peach-coloured solution was reduced in volume to *ca.* 5 mL to afford a white solid, $^{Cy}\mathbf{L_1}$, which was collected by suction filtration and dried. Yield: 0.604 g, 50%. $^{31}P\{^1H\}$ ($CDCl_3$) δ −10.2 ppm. ^1H ($CDCl_3$) δ 7.66 (d, J_{HH} 7.5, 1H, arom. H), 7.18 (t, J_{HH} 8.0, 1H, arom. H), 7.06 (d, J_{HH} 8.5, 1H, arom. H), 5.47 (d, J_{HH} 2.5, 4H, PCH_2), 3.44 (s, 3H, OMe), 1.89–1.15 (m, 44H, cy. H). FT–IR (KBr): ν_{CO} 1696 cm^{-1}. Anal. (%) Calcd. for $C_{34}H_{55}NO_3P_2$: C, 69.50; H, 9.40; N, 2.40. Found: C, 69.36; H, 9.27; N, 2.58. The deuterated analogue $^{Cy}\mathbf{L_1}^{D4}$ was similarly prepared from Cy_2PCD_2OH and used to confirm ^1H NMR methylene assignments in $^{Cy}\mathbf{L_1}$.

2.3.2. Synthesis of $Cy_2PCH_2N(Ar)CH_2PCy_2$ [Ar = $C_6H_3(1\text{-}CO_2H)(3\text{-}OH)$] $^{Cy}L_2$

3-hydroxyanthranilic acid (0.248 g, 1.62 mmol) and Cy_2PCH_2OH (0.731 g, 3.23 mmol) were dissolved in CH_3OH (20 mL) and stirred under reflux for 48 h. The resulting brown solution was evaporated to dryness, suspended in cold, degassed MeOH (5 mL) and the white solid $^{Cy}\mathbf{L_2}$ filtered and dried in vacuo. Yield: 0.694 g, 75%. $^{31}P\{^1H\}$ ($CDCl_3$) δ −12.3 ppm. ^1H [$(CD_3)_2SO$] δ 17.48 (s, 1H, COOH), 10.51 (s, 1H, OH), 7.44 (d, J_{HH} 7.6, 1H, arom. H), 7.17 (t, J_{HH} 8.0, 1H, arom. H), 7.03 (d, J_{HH} 8.4, 1H, arom. H), 3.62 (d, J_{PH} 14.4, 4H, PCH_2) 1.71–0.82 (m, 44H, cy. H). FT–IR (KBr): ν_{CO} 1634 cm^{-1}. Anal. (%) Calcd. for $C_{33}H_{53}NO_3P_2{\cdot}CH_3OH$: C, 67.40; H, 9.50; N, 2.31. Found: C, 67.82; H, 9.06; N, 2.58. The deuterated analogue $^{Cy}\mathbf{L_2}^{D4}$ was similarly prepared from Cy_2PCD_2OH and used to confirm ^1H NMR methylene assignments in $^{Cy}\mathbf{L_2}$.

2.3.3. Synthesis of $Ph_2PCH_2N(Ar)CH_2PPh_2$ [Ar = $C_6H_3(1\text{-}CO_2H)(5\text{-}OMe)$] $^{Ph}L_3$

$^{Ph}\mathbf{L_3}$ was obtained in a similar manner to $^{Cy}\mathbf{L_1}/^{Cy}\mathbf{L_2}$ from 2-amino-5-methoxybenzoic acid and Ph_2PCH_2OH in MeOH. Yield: 0.728 g, 51%. $^{31}P\{^1H\}$ [$(CD_3)_2SO$] δ −24.8 ppm. ^1H [$(CD_3)_2SO$] δ 15.30 (s, 1H, COOH), 7.75–6.80 (m, 23H, arom. H), 4.15 (s, 4H, PCH_2), 3.70 (s, 3H, OMe). Despite several attempts, an analytically pure sample for microanalysis could not be obtained.

2.3.4. Synthesis of $\{RuCl_2(\eta^6\text{-}Me_2CHC_6H_4Me)\}_2(^{Cy}L_1)$ 1a

$[RuCl(\mu\text{-}Cl)(\eta^6\text{-}Me_2CHC_6H_4Me)]_2$ (0.113 g, 0.184 mmol) and $^{Cy}\mathbf{L_1}$ (0.108 g, 0.186 mmol) were dissolved in CH_2Cl_2 (10 mL) and stirred for 5 min before reducing in volume to ~2 mL to afford a dark red solution. Slow addition of diethyl ether (10 mL) produced an orange precipitate **1a**, which was collected by suction filtration and dried in vacuo. Yield: 0.160 g, 73%. $^{31}P\{^1H\}$ NMR ($CDCl_3$) δ 40.0 ppm. ^1H ($CDCl_3$) δ 7.27 (d, 1H, $^3J_{HH}$ 8.0, arom. H), 6.95 (t, 1H, $^3J_{HH}$ 8.0, arom. H), 6.90 (d, 1H, $^3J_{HH}$ 8.5, arom. H), 5.51 (d, 4H, $^2J_{PH}$ 5.5, CH_2P), 5.47–5.29 (m, 8H, $Me_2CHC_6\mathit{H}_4Me$), 3.89 (s, 3H, OMe), 2.73 (sept, 2H, $^3J_{HH}$ 7.5, $Me_2\mathit{C}HC_6H_4Me$), 2.14–1.08 (m, 44H, Cy. H), 2.02 (s, 6H, $Me_2CHC_6H_4\mathit{Me}$), 1.21 (d, 12H, $^3J_{HH}$ 7.0, $\mathit{Me}_2CHC_6H_4Me$) ppm. FT–IR (KBr) ν_{CO} 1700 cm^{-1}. Anal. (%) Calcd. for $C_{54}H_{83}NO_3P_2Cl_4Ru_2{\cdot}CH_2Cl_2$ requires: C, 51.40; H, 6.70; N, 1.10. Found: C, 51.00; H, 6.20; N, 1.30.

2.3.5. Synthesis of $\{RuCl_2(\eta^6\text{-}Me_2CHC_6H_4Me)\}_2(^{Cy}L_2)$ 1b

$[RuCl(\mu\text{-}Cl)(\eta^6\text{-}Me_2CHC_6H_4Me)]_2$ (0.101 g, 0.165 mmol) and $^{Cy}\mathbf{L_2}$ (0.094 g, 0.17 mmol) were dissolved in CH_2Cl_2 (10 mL) and stirred for 5 min. The resulting red solution was evaporated to ~2 mL before slow addition of diethyl ether (10 mL) afforded an orange precipitate **1b**, which was collected by suction filtration and dried in vacuo. Yield: 0.136 g, 70%. $^{31}P\{^1H\}$ NMR ($CDCl_3$) indicates, in solution, facile conversion to an approx. 1:1 mixture of **2b** and **3**. FT–IR (KBr) ν_{CO} 1693 cm^{-1}. Anal. (%) Calcd. for $C_{53}H_{81}NO_3P_2Cl_4Ru_2$ requires: C, 53.70; H, 6.90; N, 1.20. Found: C, 53.90; H, 6.40; N, 0.90.

2.3.6. Synthesis of $\{RuCl_2(\eta^6\text{-}Me_2CHC_6H_4Me)\}_2(^{Ph}L_1)$ 1c

$[RuCl(\mu\text{-}Cl)(\eta^6\text{-}Me_2CHC_6H_4Me)]_2$ (0.097 g, 0.16 mmol) and $^{Ph}\mathbf{L_1}$ (0.091 g, 0.16 mmol) were dissolved in CH_2Cl_2 (10 mL) and the solution stirred for 5 mins. The volume of the solution was reduced to approx. 2 mL and slow addition of diethyl ether (10 mL) afforded an orange precipitate. The solid **1c** was collected by suction filtration and dried in vacuo. Yield: 0.167 g, 89%. Selected data for **1c**: $^{31}P\{H\}$ ($CDCl_3$) δ 19.2 ppm. ^1H ($CDCl_3$) δ 7.88 (t, J_{HH} 7.5, 4H, arom. H), 7.67 (t, J_{HH} 6.5, 4H, arom. H), 7.41–7.25 (m, 8H, arom. H), 7.15 (t, J_{HH} 7.5, 4H, arom. H), 7.10 (d, 1H, J_{HH} 7.5, arom. H), 6.67 (t, 1H, J_{HH} 8.0, arom. H), 6.14 (d, 1H, J_{HH} 7.5, arom. H.), 5.19 (d, 2H, J_{HH} 6.5, $Me_2CHC_6\mathit{H}_4Me$), 5.06, (d, 2H, J_{HH} 6.5, $Me_2CHC_6\mathit{H}_4Me$), 4.85 (d, 2H, J_{PH} 16.5, CH_2P), 4.78 (d, 2H, J_{HH} 6.5, $Me_2CHC_6\mathit{H}_4Me$), 4.62

(d, 2H, J_{HH} 6.5, $Me_2CHC_6H_4Me$), 4.42 (d, 2H, J_{PH} 16.5, CH_2P), 3.52 (s, 3H, OMe), 2.37 (sept, 2H, J_{HH} 6.0 $Me_2CHC_6H_4Me$), 1.64 (s, 6H, $Me_2CHC_6H_4Me$), 0.87 (d, 6H, J_{HH} 6.5, $Me_2CHC_6H_4Me$). FT–IR (KBr): ν_{CO} 1706 cm^{-1}. Anal. (%) Calcd. for $C_{54}H_{59}NO_3P_2Cl_4Ru_2{\cdot}CH_3OH$: C, 54.70; H, 5.30; N, 1.20. Found: C, 54.20; H, 4.90; N, 0.70.

2.3.7. Synthesis of $\{RuCl_2(\eta^6\text{-}Me_2CHC_6H_4Me)\}_2(^{Ph}L_2)$ 1d

$[RuCl(\mu\text{-}Cl)(\eta^6\text{-}Me_2CHC_6H_4Me)]_2$ (0.104 g, 0.171 mmol) and $^{Ph}\mathbf{L_2}$ (0.0941 g, 0.171 mmol) were dissolved in a mixture of CH_2Cl_2 (10 mL) and MeOH (5 mL) and stirred for 5 min. The resulting mixture was evaporated to dryness and the red, crystalline solid re-dissolved in CH_2Cl_2 (2 mL). Slow addition of diethyl ether (10 mL) produced an orange-brown precipitate **1d**, which was collected by suction filtration and dried in vacuo. Yield: 0.125 g, 63%. $^{31}P\{^1H\}$ NMR ($CDCl_3$) δ 19.1 ppm. ^1H ($CDCl_3$) δ 8.03–6.54 (m, 20H, arom. H), 5.47–4.46 (m, 8H, $Me_2CHC_6H_4Me$), 4.85 (d, 2H, $^2J_{PH}$ 16.0, CH_2P), 4.57 (d, 2H, $^2J_{PH}$ 16.0, CH_2P), 2.35 (sept, 2H, $^3J_{HH}$ 7.5, $Me_2CHC_6H_4Me$), 2.16–1.73 (m, 6H, $Me_2CHC_6H_4Me$); 1.27–0.66 (m, 12H, $Me_2CHC_6H_4Me$) ppm. FT–IR (KBr) ν_{CO} 1710 cm^{-1}. Anal. (%) Calcd. for $C_{53}H_{57}NO_3P_2Cl_4Ru_2$ requires: C, 54.80; H, 4.90; N, 1.20. Found: C, 54.50; H, 5.20; N, 0.80.

2.3.8. Synthesis of $\{RuCl_2(\eta^6\text{-}Me_2CHC_6H_4Me)\}_2(^{Ph}L_3)$ 1e

Compound **1e** was prepared in 53% yield following similar methods to **1a**–**d**. Selected data: $^{31}P\{^1H\}$ NMR ($CDCl_3$) δ 22.7 ppm. Anal. (%) Calcd. for $C_{54}H_{59}NO_3P_2Cl_4Ru_2$ requires: C, 55.15; H, 5.07; N, 1.19. Found: C, 54.47; H, 4.90; N, 1.43.

2.3.9. Synthesis of $\{RuCl_2(\eta^6\text{-}Me_2CHC_6H_4Me)\}_2(^{Ph}L_4)$ 1f

$[RuCl(\mu\text{-}Cl)(\eta^6\text{-}Me_2CHC_6H_4Me)]_2$ (0.037 g, 0.060 mmol) and $^{Ph}\mathbf{L_4}$ (0.033 g, 0.060 mmol) were dissolved in $CDCl_3$ (1 mL) whereupon solid **1f** deposited after a few minutes. The suspension was stirred for 2h and diethyl ether (15 mL) added to achieve further precipitation. The solid was collected by suction filtration and dried in vacuo. Yield: 0.063 g, 90%. Selected data: $^{31}P\{^1H\}$ NMR (CD_3OD) δ 23.0 ppm. FT–IR (KBr) ν_{CO} 1662 cm^{-1}. Anal. (%) Calcd. for $C_{53}H_{57}NO_3P_2Cl_4Ru_2$ requires: C, 54.80; H, 4.90; N, 1.20. Found: C, 54.81; H, 4.69; N, 0.63.

2.3.10. Synthesis of 2d and 2e

Typical procedures are illustrated for compounds **2d** and **2e**. For compound **2d**: A dark red solution of $[RuCl(\mu\text{-}Cl)(\eta^6\text{-}Me_2CHC_6H_4Me)]_2$ (0.032 g, 0.052 mmol) and $^{Ph}\mathbf{L_2}$ (0.028 g, 0.051 mmol) in $CDCl_3$ (1 mL) was allowed to stand at room temperature for ca. 5 d. The solid was collected by suction filtration and dried. Yield: 0.018 g, 51%. Selected data: $^{31}P\{^1H\}$ NMR ($CDCl_3/CH_3OH$) δ 23.3 ppm. FT–IR (KBr) ν_{CO} 1731 cm^{-1}. Anal. (%) Calcd. for $C_{31}H_{32}NO_3PCl_2Ru{\cdot}CDCl_3$ requires: C, 48.71; H, 4.22; N, 1.78. Found: C, 48.65; H, 4.04; N, 1.56. For compound **2e**: A $CDCl_3$ (0.7 ml) solution of **1e** (0.0085 g) was allowed to stand at room temperature for ca. 2d. Fractional crystallisation using diethyl ether gave a crystalline solid (0.0027 g) which was shown, by $^{31}P\{^1H\}$ NMR, to be a mixture of predominantly **2e** (δ 26.2, ~80%) and **4** (δ 21.6, ~20%). Other selected data [$^{31}P\{^1H\}$ NMR ($CDCl_3$)] for compounds **2a**–**2c**: δ 32.0 (**2a**); 32.6 (**2b**); 23.9 (**2c**) ppm. For **2c**: ^1H ($CDCl_3$) δ 8.02 (t, J_{HH} 7.5, 4H, arom. H), 7.37 (m, 7H, arom. H), 6.78 (t, J_{HH} 5.0, 1H, arom. H), 6.63 (d, 1H, J_{HH} 10.0, arom. H), 5.17 (d, 2H, J_{HH} 5.0, C_6H_4), 5.11, (d, 2H, J_{HH} 5.0, C_6H_4), 5.08 (d, 2H, J_{PH} 5.0, CH_2P), 4.67 (s, 2H, CH_2N), 3.40 (s, 3H, OMe), 2.45 (sept, 1H, J_{HH} 5.0 CH_3), 1.74 (s, 3H, CH_3), 0.92 (d, 6H, J_{HH} 5.0, CH_3). Anal. (%) Calcd. for $C_{32}H_{34}NO_3PCl_2Ru$: C, 56.22; H, 5.02; N, 2.05. Found: C, 55.70; H, 4.88; N, 1.89.

2.3.11. Synthesis of 6b

A $CDCl_3$ (0.7 mL) solution of $[IrCl(\mu\text{-}Cl)(\eta^5\text{-}C_5Me_5)]_2$ (0.018 g, 0.023 mmol) and $^{Ph}\mathbf{L_1}$ (0.012 g, 0.021 mmol) was heated to *ca.* 50°C, in an NMR tube, for 7 d. Monitoring by $^{31}P\{^1H\}$ revealed the clean formation of two P-species, **6b**, and $[IrCl(\eta^5\text{-}C_5Me_5)(Ph_2PH)]$ **7b**. After cooling the solution, fractional crystallisation with petroleum ether gave suitable crystals for X-ray crystallography. Yield: 0.0037 g, 21%. Selected data for **6b**: $^{31}P\{H\}$ ($CDCl_3$) δ −1.8 ppm. ^1H ($CDCl_3$) δ 7.98 (m, 4H, ArH), 7.40 (m, 7H, ArH), 6.82 (t, 1H, arom. H), 6.64 (dd, 1H, arom. H), 5.26 (d, 2H, CH_2N), 4.61 (s, 2H, CH_2P), 3.25 (s, 3H, OMe), 1.33 (d, 15H, $^4J_{PH}$ 2.0, Cp*). Anal. (%) Calcd. for $C_{32}H_{35}NO_3PCl_2Ir{\cdot}1.5CDCl_3$: C, 42.14; H, 3.86; N, 1.47. Found: C, 41.97; H, 3.68; N, 1.47. The same procedure was used for the analogous Rh^{III} compound **6a** (Yield: 0.0032 g, 20%). $^{31}P\{H\}$ ($CDCl_3$) δ 30.6 ppm, $^1J_{RhP}$ 140 Hz. ^1H ($CDCl_3$) δ 8.06 (m, 4H, ArH), 7.42 (m, 7H, ArH), 6.79 (t, 1H, arom. H), 6.62 (d, 1H, arom. H), 5.27 (d, 2H, $^2J_{PH}$ 4.0, CH_2N), 4.65 (s, 2H, CH_2P), 3.32 (s, 3H, OMe), 1.30 (d, 15H, $^4J_{PH}$ 3.6, Cp*).

2.4. X-ray crystallography

Suitable crystals of $^{Cy}\mathbf{L_1}$ were obtained by allowing a MeOH filtrate to stand for several days. Suitable crystals of **1d**·3OEt_2 and **2b** were obtained by vapour diffusion of Et_2O into a CH_2Cl_2 solution. Suitable crystals of **1f**·2$CDCl_3{\cdot}OEt_2$, **2c, 2d**·$CDCl_3$, **2e**·0.5OEt_2 and **6b**·1.5$CDCl_3$ were obtained by vapour diffusion of Et_2O into a $CDCl_3$ solution. Details of the data collection parameters and crystal data for $^{Cy}\mathbf{L_1}$, **1d**·3OEt_2, **1f**·2$CDCl_3{\cdot}OEt_2$, **2b, 2c, 2d**·$CDCl_3$, **2e**·0.5OEt_2 and **6b**·1.5$CDCl_3$ are presented in Table 1.

Measurements for $^{Cy}\mathbf{L_1}$, **1d**3OEt_2, **1f**·2$CDCl_3{\cdot}OEt_2$, **2b, 2c, 2d**·$CDCl_3$, **2e**·0.5OEt_2, and **6b**·1.5$CDCl_3$ were made on modern diffractometers using X-radiation from a rotating anode or sealed tube source [15]. Intensities were corrected for Lp effects and semi-empirically for absorption, based on symmetry-equivalent and repeated reflections [15,16]. The structures were solved [17] by direct or dual-space methods and refined on F^2 values for all unique data by full-matrix least squares [18,19]. All non-hydrogen atoms were refined anisotropically. Carbon-bound hydrogen atoms were constrained in a riding model with U_{eq} set to 1.2U_{eq} of the carrier atom (1.5 U_{eq} for methyl hydrogen). For **1d**·3OEt_2 the CO_2H group showed evidence of disorder, though this was not modelled. Despite the use of restraints there is still a rather unreliable pattern of bond lengths in this group, but the distance from O(4) to the OEt_2 strongly suggests an H-bond, and hence the correct assignment of carbonyl and hydroxyl groups. Restraints were also applied to the OEt_2 group containing O(6). For **1f**·2$CDCl_3{\cdot}OEt_2$ the hydroxyl group at O(3) is positionally disordered at either C(5) or C(7) with major occupancy of 55.9(16)% on C(7). The atoms of the Ph ring containing C(22) were modelled as disordered over two sets of positions with major occupancy 60(3)%. The two Me groups on the $\eta^6\text{-}Me_2CHC_6H_4Me$ ring containing C(51) were also modelled as two fold disordered with major occupancy 60.5(18)%, as were the atoms C(54), Cl(5) and Cl(6) in a deuterochloroform molecule with major occupancy 62(2)%. In **2b** the Me groups in the $\eta^6\text{-}Me_2CHC_6H_4Me$ ligand were modelled as 2-fold disordered with major occupancy 73.8(14)%. For **2d**·$CDCl_3$ there is a $CDCl_3$ molecule of crystallisation, modelled as having all bar the C atom split over two sets of positions with major component 56.2(16)%. For **2e**·0.5OEt_2 the OEt_2 molecule of crystallisation is disordered across a symmetry element, so was refined at exactly half weight. For **6b**·1.5$CDCl_3$ the $CDCl_3$ molecule including C(65) was modelled over two sets of positions with the C atom common to both and major occupancy 64.0(12)%. That including C(66) was also modelled as disordered over two sets of positions for the H atom and two of the three chlorines with Cl(10) common to both and major occupancy of 62(3)%.

Table 1
Crystallographic data for ^{Cy}**L$_1$**, **1d**·3OEt$_2$, **1f**·2CDCl$_3$·OEt$_2$, **2b, 2c, 2d**·CDCl$_3$, **2e**·0.5OEt$_2$ and **6b**·1.5CDCl$_3$.

Compound	^{Cy}**L$_1$**	**1d**·3OEt$_2$	**1f**·2CDCl$_3$·OEt$_2$	**2b**	**2c**	**2d**·CDCl$_3$	**2e**·0.5OEt$_2$	**6b**·1.5CDCl$_3$
Empirical formula	$C_{34}H_{51}D_4NO_3P_2$	$C_{53}H_{57}Cl_4NO_3P_2$ Ru_2·3($C_4H_{10}O$)	$C_{53}H_{56}Cl_4NO_3P_2$ Ru_2·2($CDCl_3$)·$C_4H_{10}O$	$C_{31}H_{44}Cl_2NO_3PRu$	$C_{32}H_{34}Cl_2NO_3PRu$	$C_{31}H_{32}Cl_2NO_3PRu$·$CDCl_3$	$C_{32}H_{34}Cl_2NO_3PRu$· 0.5($C_4H_{10}O$)	$C_{32}H_{35}Cl_2IrNO_3P$ ·1.5($CDCl_3$)
Formula weight	591.75	1384.23	1475.73	681.61	683.54	789.89	720.60	956.24
Crystal system	Orthorhombic	Triclinic	Triclinic	Monoclinic	Monoclinic	Triclinic	Monoclinic	Triclinic
Space group	*Pnma*	$P\bar{1}$	$P\bar{1}$	$P2_1/c$	$P2_1/c$	$P\bar{1}$	$P2_1/c$	$P\bar{1}$
a [Å]	12.83918(9)	14.1540(7)	11.960(2)	11.1749(3)	11.5086(7)	9.591(2)	14.9369(13)	9.6051(3)
b [Å]	26.82340(19)	15.0680(8)	13.769(3)	19.7445(4)	17.929(1)	10.663(3)	10.3271(9)	12.7278(4)
c [Å]	9.60069(6)	15.8022(9)	20.723(4)	14.8328(4)	15.5634(9)	17.218(4)	21.6601(19)	30.3172(10)
α [°]	90	86.720(4)	82.854(3)	90	90	95.816(4)	90	86.0066(5)
β [°]	90	74.552(5)	75.466(3)	110.740(3)	109.8956(10)	100.859(4)	100.4131(14)	87.9905(5)
γ [°]	90	82.143(4)	79.600(3)	90	90	104.132(4)	90	78.1963(5)
Volume [Å^3]	3306.39(4)	3217.2(3)	3237.8(11)	3060.67(14)	3019.6(3)	1656.8(7)	3286.1(5)	3618.3(2)
Z	4	2	2	4	4	2	4	4
λ	1.54178	1.54178	0.71073	1.54178	0.71073	0.71073	0.71073	0.71073
T [K]	100(2)	100(2)	150(2)	100(2)	150(2)	150(2)	150(2)	150(2)
Density (calcd.) [Mg /m^3]	1.189	1.429	1.514	1.479	1.504	1.583	1.457	1.755
Absorption coeff. [mm^{-1}]	1.44	6.19	0.97	6.50	0.78	0.96	0.73	4.25
Crystal habit and colour	Block, colourless	Block, red	Block, orange	Plate, orange	Block, orange	Block, orange	Plate, orange	Block, orange
Crystal size [mm^3]	0.37 × 0.18 × 0.08	0.15 × 0.10 × 0.05	0.20 × 0.16 × 0.11	0.10 × 0.04 × 0.01	0.17 × 0.16 × 0.06	0.20 × 0.14 × 0.07	0.25 × 0.16 × 0.06	0.39 × 0.23 × 0.10
θ Range [°]	4.9-68.2	3.3-68.2	1.8-25.0	3.9-68.2	1.9-29.1	2.2-26.0	1.9-25.0	1.7-29.1
Reflections collected	21307	52238	22962	27133	26627	12618	22927	32282
Independent reflections	3085	11645	11308	5582	7335	6439	5781	16775
R_{int}	0.019	0.070	0.071	0.093	0.056	0.052	0.055	0.021
Reflections with $F^2 > 2\sigma(F^2)$	3031	9491	6537	4915	4761	4800	3995	13893
Number of parameters	305	732	818	376	365	422	410	888
Largest difference peak/hole [e Å^{-3}]	0.29, −0.22	2.69, −1.11	2.70, −1.42	1.19, −0.79	0.96, −0.74	2.90, −1.70	2.08, −0.74	1.26, −1.05
Final R^a, $R_w{}^b$	0.028, 0.069	0.066, 0.180	0.077, 0.249	0.049, 0.126	0.042, 0.089	0.072, 0.201	0.064, 0.184	0.026, 0.062

[a] $R = \Sigma||Fo| - |Fc||/\Sigma|Fo|$. [b] $wR2 = [\Sigma[w(Fo^2 - Fc^2)^2]/\Sigma[w(Fo^2)^2]]^{1/2}$.

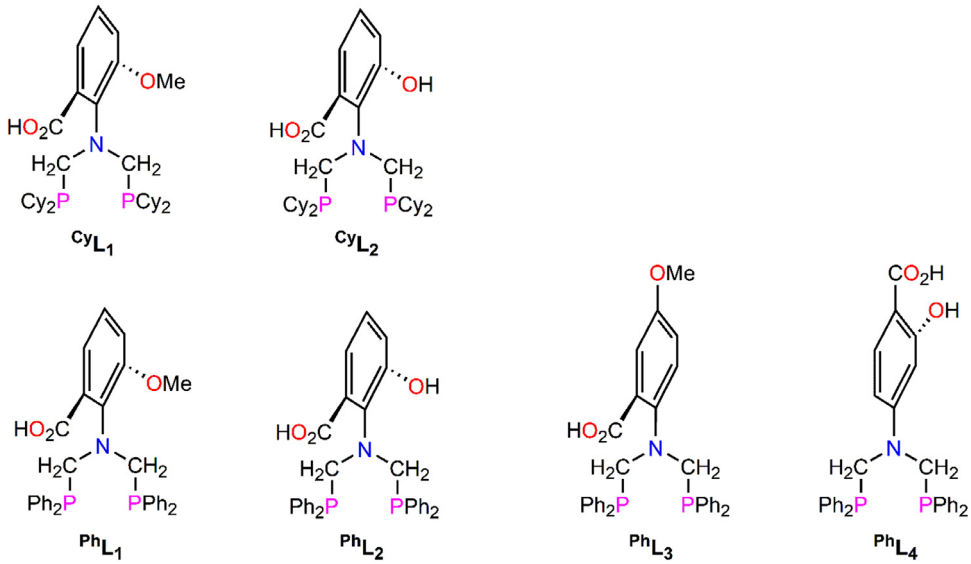

Chart 2. Ligands used in this study

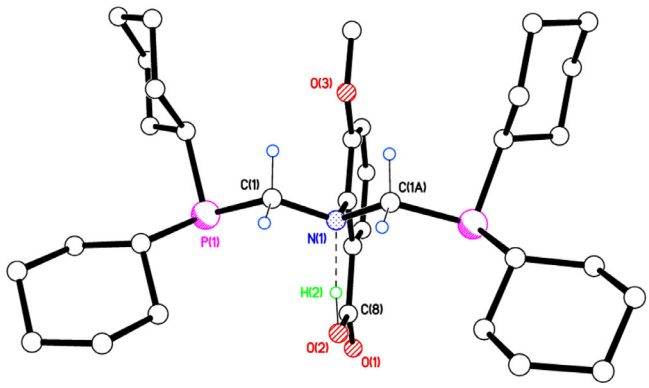

Fig. 1. Molecular structure of ligand $^{Cy}L_1$. All hydrogen atoms except on O(2) and the deuterium atoms on C(1) and C(1A) have been omitted for clarity. Selected bond lengths (Å) and angles (°): P(1)–C(1) 1.8661(11), C(1)–N(1) 1.4906(12), C(8)–O(1) 1.218(2), C(8)–O(2) 1.317(2). P(1)–C(1)–N(1) 113.67(7).

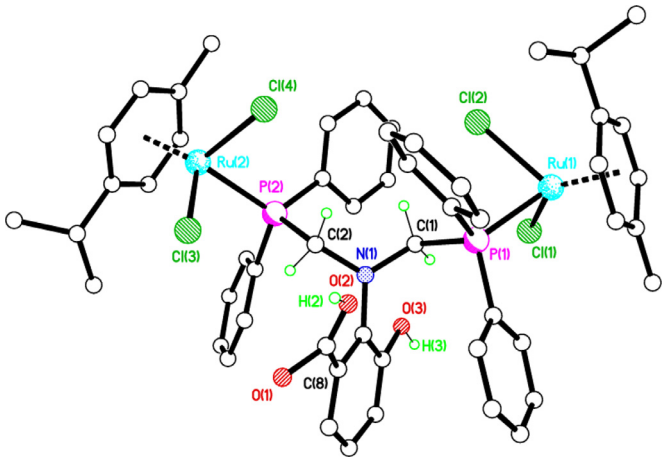

Fig. 2. Molecular structure of **1d**•3OEt$_2$. All solvent molecules of crystallisation and hydrogen atoms, except on C(1), C(2), O(2), and O(3), have been omitted for clarity. Selected bond lengths (Å) and angles (°): Ru(1)–Cl(1) 2.4175(14), Ru(1)–Cl(2) 2.4084(14), Ru(1)–P(1) 2.3555(15), Ru(2)–Cl(3) 2.4065(15), Ru(2)–Cl(4) 2.4110(16), Ru(2)–P(2) 2.3476(15), C(9)–O(1) 1.335(11), C(9)–O(2) 1.162(11). Cl(1)–Ru(1)–Cl(2) 88.70(5), Cl(1)–Ru(1)–P(1) 88.77(5), Cl(2)–Ru(1)–P(1) 83.23(5), Cl(3)–Ru(2)–Cl(4) 87.84(5), Cl(3)–Ru(2)–P(2) 86.55(5), Cl(4)–Ru(2)–P(2) 85.73(5).

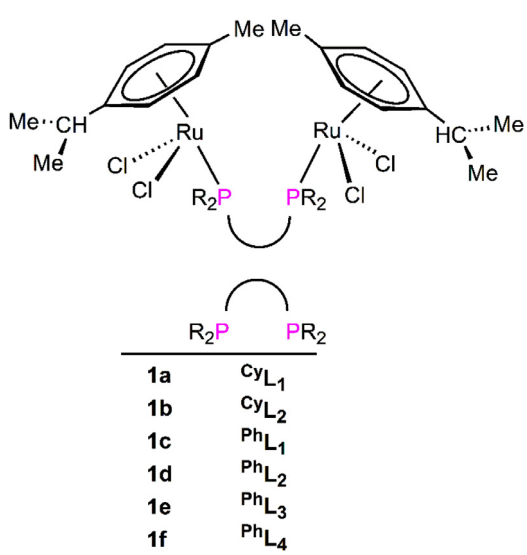

Chart 3. Diruthenium complexes **1a–f** prepared in this study.

3. Results and discussion

3.1. Ligand synthesis

Using a well-established Mannich procedure [6] reaction of 1 equiv. of the appropriate amine and 2 equiv. of either Ph_2PCH_2OH (for $^{Ph}L_3$) or Cy_2PCH_2OH ($^{Cy}L_1$, $^{Cy}L_2$) in MeOH afforded the new carboxylic acid functionalised diphosphines in good yield (Chart 2). Characterising data (see Experimental section) for $^{Ph}L_3$, $^{Cy}L_1$, and $^{Cy}L_2$ are in good agreement with the proposed structures. The $^{31}P\{^1H\}$ NMR spectra show typical singlets at δ(P) −10.2 ($^{Cy}L_1$), −12.3 ($^{Cy}L_2$) and −25.6 ($^{Ph}L_3$) ppm. The ^1H NMR spectra are particularly diagnostic showing, in addition to the expected resonances for the Ph/Cy groups, resonances at δ(H) 16.3 and 16.0 ppm (CO_2H) and the CH_2 protons appear as an AB splitting pattern at δ(H) 4.18 ppm, consistent with inequivalence of the two methylene protons, presumably imposed by orientation of the N-bound arene group which is perpendicular (for $^{Ph}L_1$) [6e]. In $^{Ph}L_2$ the CH_2 pro-

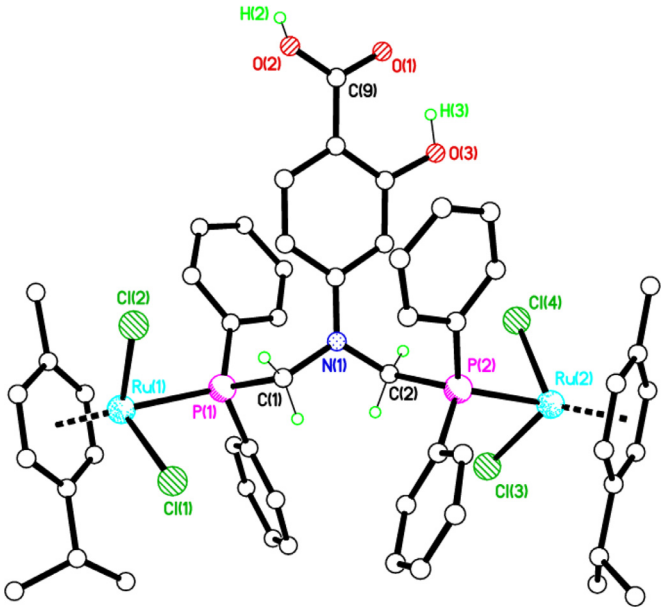

Fig. 3. Molecular structure of **1f**·2CDCl$_3$·OEt$_2$. All solvent molecules of crystallisation and hydrogen atoms, except on C(1), C(2), O(2), and O(3), have been omitted for clarity. Selected bond lengths (Å) and angles (°): Ru(1)–Cl(1) 2.417(3), Ru(1)–Cl(2) 2.403(2), Ru(1)–P(1) 2.344(2), Ru(2)–Cl(3) 2.410(3), Ru(2)–Cl(4) 2.413(2), Ru(2)–P(2) 2.337(2), C(9)–O(1) 1.272(11), C(9)–O(2) 1.290(11). Cl(1)–Ru(1)–Cl(2) 87.05(10), Cl(1)–Ru(1)–P(1) 83.50(8), Cl(2)–Ru(1)–P(1) 86.75(8), Cl(3)–Ru(2)–Cl(4) 88.14(9), Cl(3)–Ru(2)–P(2) 83.67(9), Cl(4)–Ru(2)–P(2) 85.34(8).

tons appear as a singlet at 4.27 ppm [6e]. Deuterium analogues of ^{Cy}**L$_1$**, ^{Cy}**L$_2$**, ^{Ph}**L$_1$**, and ^{Ph}**L$_2$**, labelled with deuterium on the methylene carbons, were similarly prepared [20].

The X-ray structure of ^{Cy}**L$_1$** has been determined and is shown in Fig. 1. The molecular structure confirms diphosphine formation and a P–C–N–C–P arrangement with a near perpendicular N-arene group [torsion angle 88.74(3)°]. The P–C and C–N bond lengths are similar to those previously reported [6e] for ^{Ph}**L$_1$** and there is a strong N(1)···H(2)–O(2) [N(1)···O(2) 2.5201(16) Å, 161(2)°] intramolecular H bond. The molecule lies on a mirror plane.

3.2. Dinuclear ruthenium(II) complexes *1a–f*

Reaction of ligands ^{Cy}**L$_1$**–^{Ph}**L$_4$** with [RuCl(μ-Cl)(η^6-Me$_2$CHC$_6$H$_4$Me)]$_2$ (1:1 ratio) in CH$_2$Cl$_2$ gave, after workup, orange solids **1a–f** in 48–89% isolated yields (Chart 3). All compounds were characterised by NMR spectroscopy whereby ^{31}P{^{1}H} NMR downfield shifts were consistent with bridging P-coordination of these ligands. When CDCl$_3$ solutions of **1a–e** were monitored over several days, two major new Ru^{II} phosphorus compounds were observed, both of which have been identified (vide infra).

Whilst diphosphines of this structural motif can P/P-chelate to ruthenium metal centres [21], the molecular structure of **1d**·3OEt$_2$ (Fig. 2) confirms a binuclear arrangement comprising two pseudo-tetrahedral {RuCl$_2$(η^6-Me$_2$CHC$_6$H$_4$Me)} fragments and a bridging ^{Ph}**L$_2$** ligand [22]. The Ru^{II} to ring centroid distances are very similar at 1.694(2) Å at Ru(1), and 1.699(3) Å at Ru(2), with a piano-stool conformation around each Ru metal centre. Unlike ^{Cy}**L$_1$** and ^{Ph}**L$_1$** [6e], the N-arene group torsion angle observed with respect to the C(1)–N(1)–C(2) plane in **1d**·3OEt$_2$ is 47.7(3)° whilst in **1f**·2CDCl$_3$·OEt$_2$ this group is essentially parallel [0.8(11)°]. In **1d**·3OEt$_2$ both the hydroxyl and carboxylic acid hydrogens act as H-bond donors to OEt$_2$ molecules of crystallisation (see ESI Fig. S1).

The molecular structure of **1f**·2CDCl$_3$·OEt$_2$ (Fig. 3) confirms a binuclear arrangement comprising two pseudo-tetrahedral {RuCl$_2$)(η^6-Me$_2$CHC$_6$H$_4$Me} fragments and a bridging ^{Ph}**L$_3$** ligand. The Ru–P and Ru–Cl bond parameters are as anticipated. Adjacent molecules form H-bonded dimers via a classic carboxylic acid head-to-tail arrangement through O(2)–H(2)···O(1A) [2.610(8) Å, 123°] hydrogen bonding. At the end of each molecule a CDCl$_3$ molecule of crystallisation forms a bifurcated H-bond to the two Ru-bound chloride ligands (see ESI Figs. S2 & S3).

3.3. Mononuclear metal complexes *2a–e*

Previously, we have shown that ligands ^{Ph}**L$_1$**, ^{Ph}**L$_2$** and ^{Ph}**L$_4$** react with the square planar complex [Pd(Me)Cl(η^4-cod)] to form novel Pd$_6$ hexameric compounds via P/P/O-tridentate coordination [6e]. In these complexes, ^{Ph}**L$_1$**, ^{Ph}**L$_2$** and ^{Ph}**L$_4$** act as P/P-chelating ligands to Pd^{II} and protonation of the Me group, by the -CO$_2$H, results in carboxylate formation link-

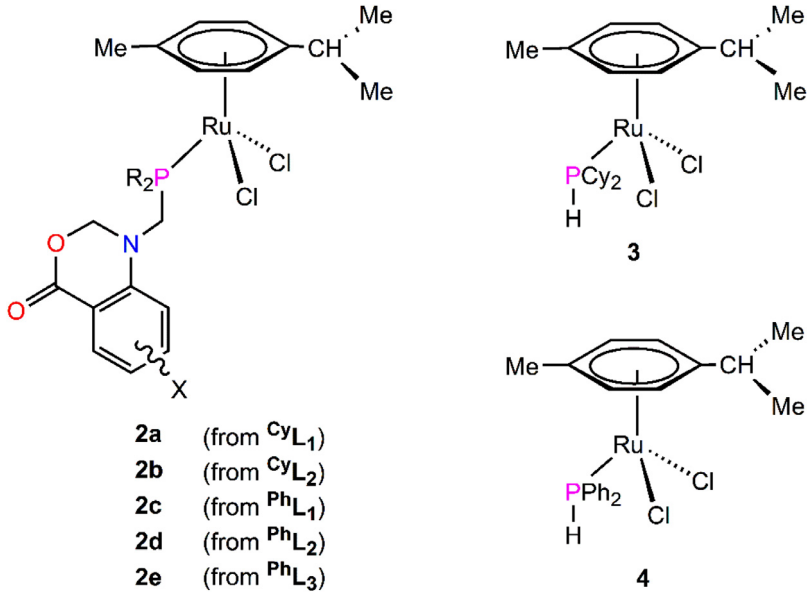

Chart 4. Chemical structures of **2a-e**, **3**, and **4**.

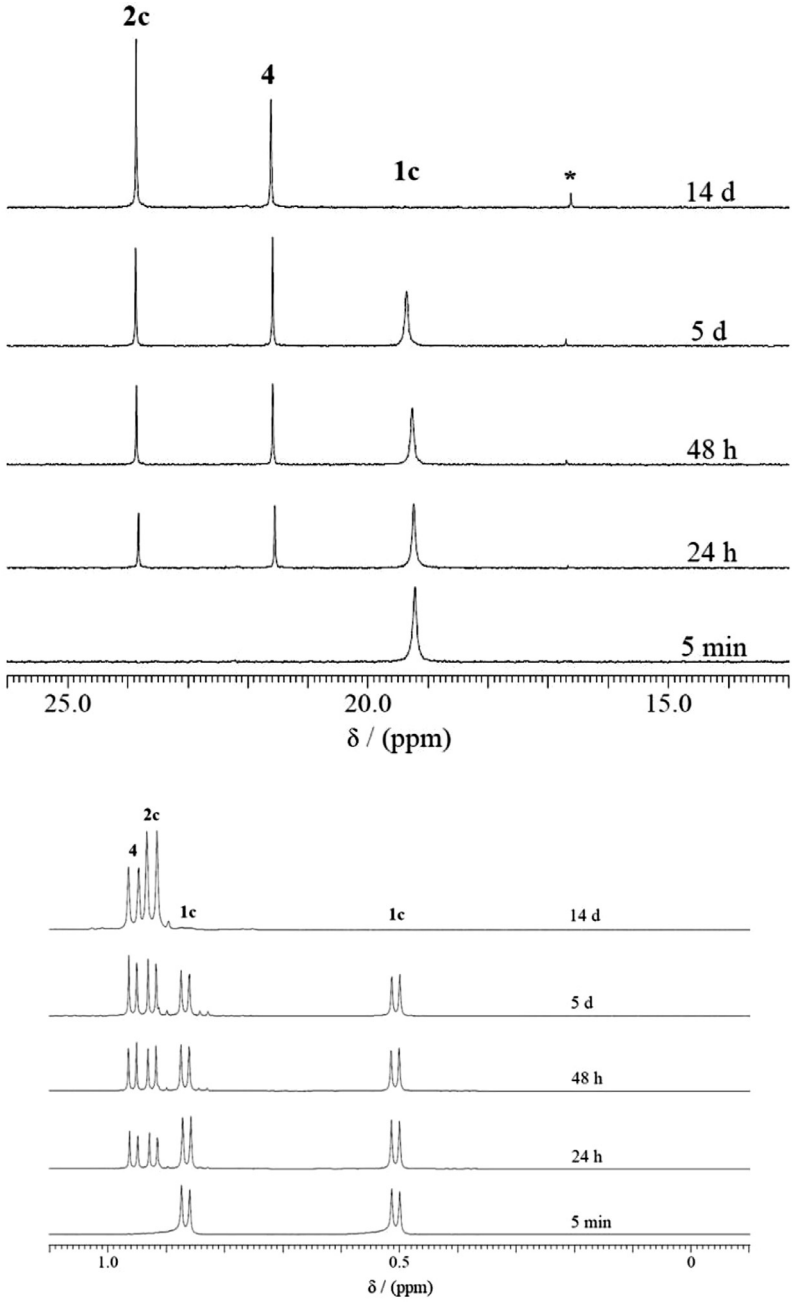

Fig. 4. (upper) $^{31}P\{^1H\}$ NMR spectra (in $CDCl_3$) showing P–C(sp^3) cleavage of **1c** over time. The minor species at around 17 ppm is probably [Ru(η^6-$Me_2CHC_6H_4Me$)Cl_2(Ph_2PCH_2OH)] [6g]. (lower) ^1H NMR spectra (selected region) showing P– C(sp^3) cleavage of **1c** over time.

ing Pd^{II} units into hexamers. In contrast, when $CDCl_3$ solutions of compounds **1a**–**e** were left at r.t. or gently heated, smooth conversion to two new P-containing Ru^{II} compounds in approx. 1:1 ratio was observed. These were identified as **2a**–**e** (Chart 4) and either [Ru(η^6-$Me_2CHC_6H_4Me$)Cl_2(Cy_2PH)] **3** or [Ru(η^6-$Me_2CHC_6H_4Me$)Cl_2(Ph_2PH)] **4** [23,24]. The progress of these reactions was easily monitored by $^{31}P\{^1H\}$ (Fig. 4, upper) and ^1H NMR (Fig. 4, lower) spectroscopy. The identity of both **3** and **4** could be confirmed, in $CDCl_3$, by the diagnostic $^1J_{PH}$ coupling (409 Hz) which was not observed in the known compound [Ru(η^6-$Me_2CHC_6H_4Me$)Cl_2(Ph_2POH)], demonstrating that no Ph_2PH dissociation, P^{III} to P^V oxidation and re-coordination as Ph_2POH to the Ru^{II} centre had taken place [24]. Furthermore, ^1H NMR spectra (Fig. 4, lower), recorded over the same time period, could also be used to monitor this clean conversion as evidenced by the $Me_2CHC_6H_4Me$ protons.

Under similar concentrations, monitoring the P–C(sp^3) bond cleavage across the series **1a**–**e** reveals that this process occurs within 1 d (at r.t.) for **1a** and slowest (14 d) for **1c**, reflecting the importance of the different electronic effects of Cy and Ph substituents on P respectively. The N-arene functionality (OMe *vs* OH) also plays a significant role, as demonstrated by **1b** which underwent P–C(sp^3) bond cleavage completely within 8 h (at r. t.). It should also be noted that the overall disposition of substituents on the N-arene ring may help contribute towards imposing the dinuclear ruthenium complex into one preferred conformer that favours P–C(sp^3) bond cleavage. C–H activation of a methylene hydrogen has previously been reported in two Fe and Mo complexes bearing a di/triphosphine based on a P–C–N–C–P framework [25].

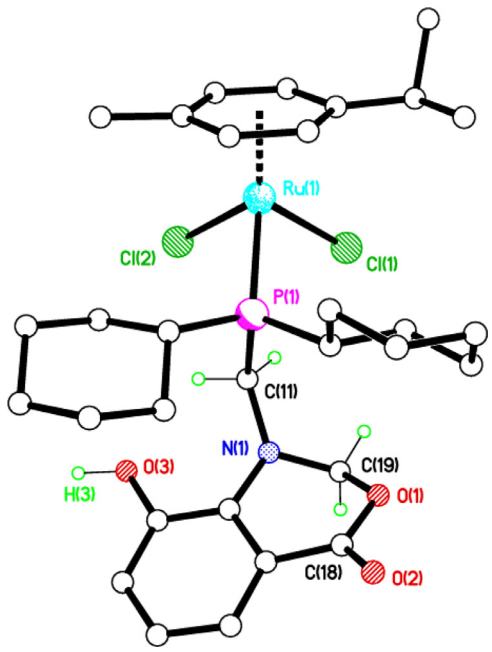

Fig. 5. Molecular structure of **2b**. All hydrogen atoms, except on C(11), C(19) and O(3), have been omitted for clarity. Selected bond lengths (Å) and angles (°): Ru(1)–Cl(1) 2.4165(10), Ru(1)–Cl(2) 2.4269(10), Ru(1)–P(1) 2.3860(11), C(18)–O(1) 1.356(5), C(18)–O(2) 1.211(5). O(1)–C(19) 1.462(5), Cl(1)–Ru(1)–Cl(2) 86.51(4), Cl(1)–Ru(1)–P(1) 86.54(3), Cl(2)–Ru(1)–P(1) 86.65(3).

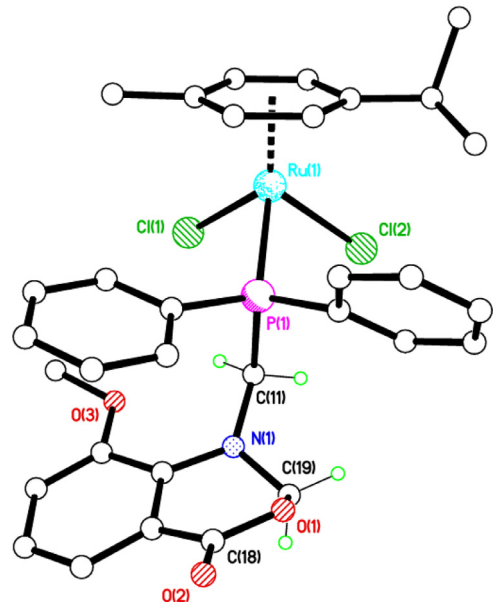

Fig. 6. Molecular structure of **2c**. All hydrogen atoms except on C(11) and C(19) have been omitted for clarity. Selected bond lengths (Å) and angles (°): Ru(1)–Cl(1) 2.4227(9), Ru(1)–Cl(2) 2.4152(9), Ru(1)–P(1) 2.3507(10), C(18)–O(1) 1.351(5), C(18)–O(2) 1.209(4), O(1)–C(19) 1.450(4). Cl(1)–Ru(1)–Cl(2) 89.56(3), Cl(1)–Ru(1)–P(1) 88.09(3), Cl(2)–Ru(1)–P(1) 83.67(3).

Compounds **2a**–**e** could generally be separated by fractional crystallisation and the structures of four examples were determined by X-ray crystallography (Figs. 5–8). Important bond lengths and angles are given in the Fig. captions. Each of the complexes displays a typical three-legged piano stool structure with Ru–P and Ru–Cl bond distances broadly as anticipated [6g,23,26]. Suitable crystals of **2b** were obtained by vapour diffusion of Et_2O into a CH_2Cl_2 solution. The molecular structure of **2b** (Fig. 5) confirms a mononuclear arrangement comprising a piano-stool {$RuCl_2(\eta^6$-$Me_2CHC_6H_4Me)$} metal fragment and a monodentate P-ligand containing a six membered N(1)–C(12)–C(13)–C(18)–O(1)–C(19) heterocyclic lactone. The Ru to ring centroid distance is 1.7098(17) Å. Molecules of **2b** form H-bonded dimers via centrosymmetric pairs of head-to-tail O–H···Cl hydrogen bonds (see ESI Fig. S4).

Compounds **2b** and **2c** are pseudo-isomorphous, both crystallising in space group $P2_1/c$ with fairly similar unit cell dimensions. (see Table 1) The molecular structure of **2c** (Fig. 6) confirms a mononuclear arrangement comprising a piano-stool {$RuCl_2(\eta^6$-$Me_2CHC_6H_4Me)$} metal fragment and a monodentate P-ligand containing a six-membered N(1)–C(12)–C(13)–C(18)–O(1)–C(19) lactone ring as observed in **2b**. The Ru–P and Ru–Cl bond parameters are broadly as anticipated. The Ru(1)–$C_{centroid}$ distance is 1.6974(14) Å.

The molecular structure of **2d**·$CDCl_3$ (Fig. 7) confirms a mononuclear arrangement comprising a piano-stool {$RuCl_2(\eta^6$-$Me_2CHC_6H_4Me)$} metal fragment and a monodentate P-ligand containing a six-membered N(1)–C(12)–C(13)–C(18)–O(1)–C(19) heterocyclic lactone as seen for **2b** and **2c**. The Ru–P and Ru–Cl bond parameters are broadly as anticipated and the Ru(1)–$C_{centroid}$ distance is 1.704(3) Å. The hydroxy group forms an intramolecular O(3)–H(3)···N(1) [2.846(7) Å, 122(8)°Å] hydrogen bond which differs from the intermolecular H-bond interactions seen in **2b**.

The molecular structure of **2e**·0.5OEt_2 (Fig. 8) confirms a mononuclear arrangement comprising the familiar piano-stool {$RuCl_2(\eta^6$-$Me_2CHC_6H_4Me)$} metal fragment

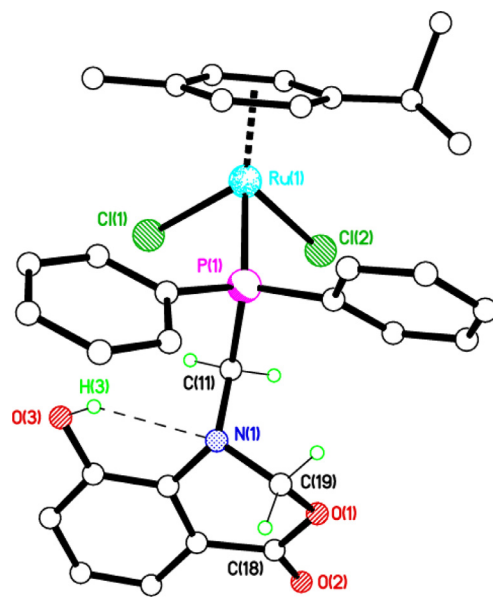

Fig. 7. Molecular structure of **2d**·$CDCl_3$. The solvent molecule of crystallisation and hydrogen atoms, except on C(11), C(19), and O(3), have been omitted for clarity. Selected bond lengths (Å) and angles (°): Ru(1)–Cl(1) 2.4229(16), Ru(1)–Cl(2) 2.4083(16), Ru(1)–P(1) 2.3471(17), C(18)–O(1) 1.353(9), C(18)–O(2) 1.219(8), O(1)–C(19) 1.460(8). Cl(1)–Ru(1)–Cl(2) 87.31(6), Cl(1)–Ru(1)–P(1) 87.21(5), Cl(2)–Ru(1)–P(1) 85.00(6).

and a monodentate P-ligand containing a six-membered N(1)–C(12)–C(13)–C(18)–O(1)–C(19) heterocyclic lactone as seen previously and demonstrating the universality of this transformation. The Ru–P and Ru–Cl bond parameters are broadly as anticipated and the Ru(1)–$C_{centroid}$ distance is 1.694(3) Å, all in accord with the previous three Ru structures. Adjacent molecules form weakly H-bonded centro-symmetric dimer pairs via pairs of η^6-$Me_2CHC_6H_4Me$ (CH)···Cl′ interactions (see ESI Fig. S5).

We also briefly explored the scope of this transformation with other dinuclear chloro-bridged late transition metal centres. Us-

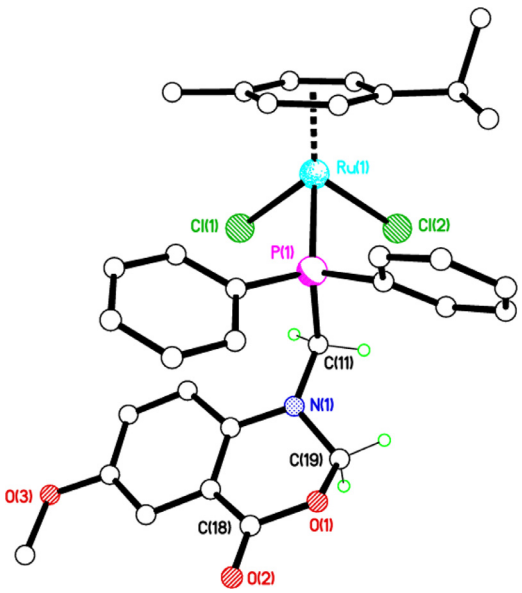

Fig. 8. Molecular structure of **2e**·0.5OEt$_2$. All solvent molecules of crystallisation and hydrogen atoms, except on C(11) and C(19), have been removed for clarity. Selected bond lengths (Å) and angles (°): Ru(1)–Cl(1) 2.418(2), Ru(1)–Cl(2) 2.4049(19), Ru(1)–P(1) 2.3435(18), C(18)–O(1) 1.409(12), C(18)–O(2) 1.239(11), O(1)–C(19) 1.425(10). Cl(1)–Ru(1)–Cl(2) 88.78(7), Cl(1)–Ru(1)–P(1) 85.47(6), Cl(2)–Ru(1)–P(1) 83.59(6).

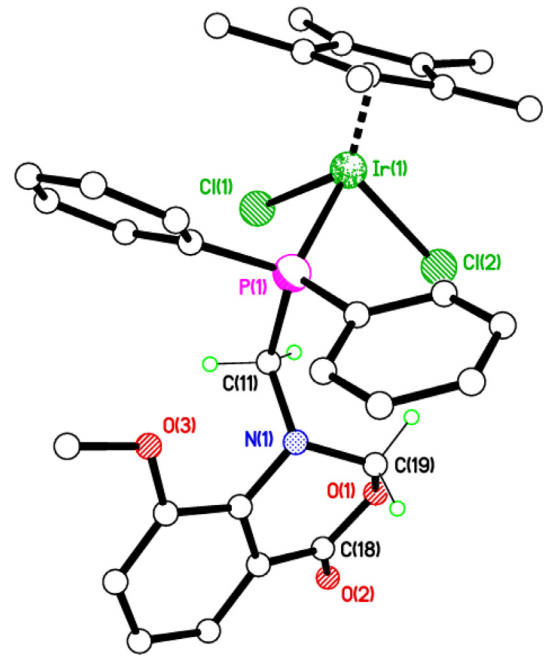

Fig. 9. Molecular structure of **6b**·1.5CDCl$_3$. All solvent molecules of crystallisation and hydrogen atoms, except on C(11) and C(19), have been omitted for clarity. Selected bond lengths (Å) and angles (°) (values for second independent molecule in parenthesis): Ir(1)–Cl(1) 2.4188(8) [2.4150(8)], Ir(1)–Cl(2) 2.4194(8) [2.3995(8)], Ir(1)–P(1) 2.3043(8) [2.3174(8)], C(18)–O(1) 1.353(4) [1.349(5)], C(18)–O(2) 1.211(4) [1.219(4)], O(1)–C(19) 1.463(4) [1.465(4)]. Cl(1)–Ir(1)–Cl(2) 89.04(3) [88.89(3)], Cl(1)–Ir(1)–P(1) 86.96(3) [89.07(3)], Cl(2)–Ir(1)–P(1) 87.81(3) [87.64(3)].

ing ^{Ph}**L$_1$**, reaction with [RhCl(μ-Cl)(η^5-C$_5$Me$_5$)]$_2$ (1:1) in CH$_2$Cl$_2$, and precipitation with Et$_2$O/pet. ether (b.p. 60-80 °C), gave a solid which was analysed by ^{31}P{^{1}H} NMR as a 50:50 mixture of **6a** (Chart 5) [30.2 ppm, J_{RhP} 145 Hz] and [RhCl$_2$(η^5-C$_5$Me$_5$)(Ph$_2$PH)] **7a** [13.6 ppm, J_{RhP} 141 Hz] [24,27] with no evidence for **5a**. When this reaction was monitored in CDCl$_3$, by ^{31}P{^{1}H} NMR over time (ca. 4 d, 50 °C), initial formation of the binuclear Rh^{III} complex **5a** [29.4 ppm, J_{RhP} 137 Hz] was observed followed by slow conversion into **6a** [30.7 ppm, J_{RhP} 141 Hz] and **7a** [14.0 ppm, J_{RhP} 142 Hz] [27]. Furthermore, when [IrCl(μ-Cl)(η^5-C$_5$Me$_5$)]$_2$ and ^{Ph}**L$_1$** (1:1) were mixed in CDCl$_3$, the binuclear complex **5b** [δ(P) −4.2 ppm] was immediately formed. The ^{1}H NMR spectrum showed a characteristic AX pattern for the P–CH$_2$–N methylene protons [δ(H) 5.09 and 4.58 ppm (J_{HH} 13.2 Hz) indicating significantly different environments. After standing the NMR solution for ca. 5 d at r.t., two minor species at δ(P) −2.2 and −10.2 ppm were observed, the latter assigned as the known [24] compound [IrCl$_2$(η^5-C$_5$Me$_5$)(Ph$_2$PH)] **7b**. The former we assign to **6b**. This process can be accelerated by heating a solution for 2 d, resulting in clean conversion to **6b:7b** in a 1:1 ratio. Fractional crystallisation afforded suitable orange crystals of **6b** for a single crystal X-ray structure analysis and enabled further characterisation by NMR and elemental analyses.

The molecular structure of **6b**·1.5CDCl$_3$ (Fig. 9) confirms a mononuclear arrangement comprising a piano stool IrCl$_2$(η^5-C$_5$Me$_5$) metal fragment and a monodentate P-ligand containing a six membered N(1)–C(12)–C(13)–C(18)–O(1)–C(19) heterocyclic lactone, as previously observed for the Ru^{II} examples and demonstrating cross-transition metal applicability. The Ir–P and Ir–Cl bond parameters are broadly as anticipated and the Ir(1)–C$_{centroid}$ distance is 1.8205(13) Å [Ir(2)–C$_{centroid}$ distance is 1.8192(14) Å in a second independent molecule]. There are notable differences between the two Ir complexes in the asymmetric unit and their intramolecular H-bonds between the C(11/43)H$_2$ group and the Ir-

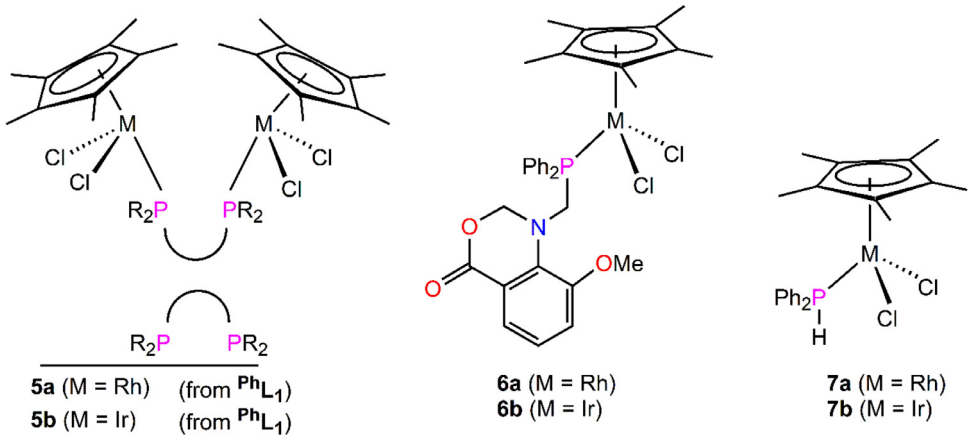

Chart 5. Chemical structures of compounds **5a**/**b**, **6a**/**b**, and **7a**/**b**.

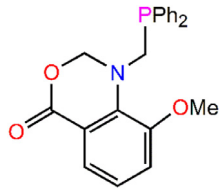

8

Chart 6. Chemical structure of **8**.

coordinated chloride ligands, and also the weak H-bonds between the metal complex molecules and the molecules of crystallisation (see ESI Figs S6 – S9).

Finally, as a control experiment, we heated under similar conditions $^{Ph}\mathbf{L_1}$ [δ(P) −22.3 ppm] in deoxygenated $CDCl_3$ and monitored this solution by $^{31}P\{^1H\}$ NMR spectroscopy. After 48 h, there was evidence of some conversion to **8** (Chart 6) [δ(P) −20.5 ppm] and Ph_2PH [δ(P) −40.0 ppm] in addition to some decomposition products including P^V oxides of both **8** and Ph_2PH. Nonetheless, this result shows that, even in the absence of a Ru^{II} metal centre, P-C(sp^3) cleavage does occur albeit leading to mixtures of several poorly defined phosphorus species. No attempts to either optimise/scope this transformation nor isolate **8** have been undertaken.

4. Conclusions

In summary, we have shown how chelating diphosphines bearing a versatile P−C−N−C−P scaffold can undergo facile P−C(sp^3) bond cleavage upon intramolecular protonation to generate a novel type of heterocyclic lactone-functionalised tertiary phosphine. This unusual transformation has been observed in several binuclear Ru^{II} complexes and their corresponding chloro-bridged Rh^{III} and Ir^{III} analogues. As a final remark, it should be highlighted that careful consideration of the stereoelectronic effects of the alkyl/aryl groups on P and the N-R group, for this class of diphosphine, is necessary to circumvent unexpected reaction pathways from taking place.

Declaration of Competing Interest

The authors declare that they have no known competing financial interests or personal relationships that could have appeared to influence the work reported in this paper.

Acknowledgements

We thank the EPSRC Centre for Doctoral Training in Embedded Intelligence under grant reference EP/L014998/1 for financial support (PD). Johnson Matthey are acknowledged for their kind donation of precious metals and the UK National Crystallography Service at the University of Southampton for three of the data collections.

Supplementary materials

Supplementary material associated with this article can be found, in the online version, at doi:10.1016/j.jorganchem.2021.121704.

Appendix A. Supplementary material

A complete set of X-ray crystallographic structural data for compounds $^{Cy}\mathbf{L_1}$, **1c**·3OEt$_2$, **1f**·2CDCl$_3$·OEt$_2$, **2b, 2c, 2d**·CDCl$_3$, **2e**·0.5OEt$_2$ and **6b**·1.5CDCl$_3$ (CCDC 2022153-60) are available free of charge via http://www.ccdc.cam.ac.uk/data_request/cif or from the Cambridge Crystallographic Data Centre, 12 Union Road, Cambridge, CB2 1EZ, UK; fax: (+44) 1223 336 033 or e-mail: deposit@ccdc.cam. ac.uk. Additional figures for several of the crystal structures are also presented.

References

[1] P.E. Garrou, Chem. Rev. 85 (1985) 171–185.
[2] T.J. Geldbach, P.S. Pregosin, Eur. J. Inorg. Chem. (2002) 1907–1918.
[3] For recent examples of P–C_{aryl} cleavage at a metal bound monodentate phosphine, see.
[(a)] A. Berkefeld, M. Reimann, G. Hörner, M. Kaupp, H. Schubert, Organometallics 39 (2020) 443–452.
[(b)] M.K. Cybulski, C.J.E. Davies, J.P. Lowe, M.F. Mahon, M.K. Whittlesey, Inorg. Chem. 57 (2018) 13749–13760.
[(c)] K.Q. Almeida Leñero, Y. Guari, P.C.J. Kamer, P.W.N.M. van Leeuwen, B. Donnadieu, S. Sabo-Etienne, B. Chaudret, M. Lutz, A.L. Spek, Dalton Trans 42 (2013) 6495–6512.
[4] For recent examples of P–C_{alkyl} cleavage at a metal bound diphosphine, see.
[(a)] S. Zhang, H. Li, A.M. Appel, M.B. Hall, R.M. Bullock, Organometallics 39 (2020) 3306–3314.
[(b)] P.M. Scheetz, D.S. Glueck, A.L. Rheingold, Organometallics 36 (2017) 3387–3397.
[(c)] S. Zhang, H. Li, A.M. Appel, M.B. Hall, R.M. Bullock, Chem. Eur. J. 22 (2016) 9493–9497.
[(d)] J. Campos, U. Hintermair, T.P. Brewster, M.K. Takase, R.H. Crabtree, ACS Catal. 4 (2014) 973–985.
[(e)] R. Quesada, J. Ruiz, V. Riera, S. García-Granda, M.R. Díaz, Chem. Commun. (2003) 1942–1943.
[5] For recent examples of P–C_{aryl} cleavage at a metal bound chelating diphosphine, see.
[(a)] C.G. Werncke, I. Müller, Chem. Commun. 56 (2020) 2268–2271.
[(b)] S. Syaida Sirat, O. Bin Shawkataly, I. Abdul Razak, Polyhedron 155 (2018) 493–499.
[6] [(a)] B. Cao, M.R.J. Elsegood, N. Lastra-Calvo, M.B. Smith, J. Organomet. Chem. 853 (2017) 159–167; [(b)] M.R.J. Elsegood, A.J. Lake, M.B. Smith, Dalton Trans (2009) 30–32; [(c)] G.M. Brown, M.R.J. Elsegood, A.J. Lake, N.M. Sanchez-Ballester, M.B. Smith, T.S. Varley, K. Blann, Eur. J. Inorg. Chem. (2007) 1405–1414; [(d)] M.B. Smith, S.H. Dale, S.J. Coles, T. Gelbrich, M.B. Hursthouse, M.E. Light, P.N. Horton, CrystEngCommun 9 (2007) 165–175; [(e)] M.R.J. Elsegood, M.B. Smith, P.M. Staniland, Inorg. Chem. 45 (2006) 6761–6770; [(f)] M.B. Smith, S.H. Dale, S.J. Coles, T. Gelbrich, M.B. Hursthouse, M.E. Light, CrystEngCommun 8 (2006) 140–149; [(g)] S.E. Dann, S.E. Durran, M.R.J. Elsegood, M.B. Smith, P.M. Staniland, S. Talib, S.H. Dale, J. Organomet. Chem. 691 (2006) 4829–4842.
[7] Y.-P. Zhang, M. Zhang, X.-R. Chen, C. Lu, D.J. Young, Z.-G. Ren, J.-P. Lang, Inorg. Chem. 59 (2020) 1038–1045.
[8] M.K. Pandey, H.S. Kunchur, D. Mondal, L. Radhakrishna, B.S. Kote, M.S. Balakrishna, Inorg. Chem. 59 (2020) 3642–3658.
[9] S. Lounissi, J.-F. Capon, F. Gloaguen, F. Matoussi, F.Y. Pétillon, P. Schollhammer, J. Talarmin, Organometallics 29 (2010) 1296–1301.
[10] [(a)] M. Plotek, R. Starosta, U.K. Komarnicka, A. Skórska-Stania, P. Kotoczek, K. Dudek, A. Kyziol, J. Mol. Struct. 1121 (2016) 104–110; [(b)] M. Plotek, R. Starosta, U.K. Komarnicka, A. Skórska-Stania, G. Stochel, A. Kyziol, M. Jezowska-Bojczuk, RSC Adv 5 (2015) 2952–2955.
[11] [(a)] R.M. Bullock, G.M. Chambers, Phil. Trans. R. Soc. A 375 (2017) 0002; [(b)] R.M. Bullock, M.L. Helm, Acc. Chem. Res. 48 (2015) 2017–2026.
[12] H. Hellmann, J. Bader, H. Birkner, O. Schumacher, Justus Liebigs Ann. Chem. 659 (1962) 49–63.
[13] M.A. Bennett, T.N. Huang, T.W. Matheson, A.R. Smith, Inorg. Synth. 21 (1982) 74–78.
[14] C. White, A. Yates, P.M. Maitlis, Inorg. Synth. 29 (1992) 228–234.
[15] [(a)] APEX II Program for Diffractometer Control, Bruker AXS Inc., Madison, WI, 2014 2006; [(b)] CrysAlis PRO, Rigaku Oxford Diffraction, 2015; [(c)] CrysAlis PRO, Agilent Technologies, 2013.
[16] [(a)] SAINT software for CCD diffractometers, Bruker AXS Inc., Madison, WI, 2014. (2006); [(b)] L. Krause, R. Herbst-Irmer, G.M. Sheldrick, D.J. StalkeSADABS software, 2015 Appl. Cryst., 48 3–10.
[17] [(a)] G.M. Sheldrick, Acta Crystallogr. Sect. 71 (2015) 3–8; [(b)] G.M. Sheldrick, Acta Crystallogr. Sect. 64 (2008) 112–122.
[18] G.M. Sheldrick, Acta Crystallogr. Sect. 71 (2015) 3–8.
[19] G.M. Sheldrick, SHELXTL user manual, Bruker AXS Inc., Madison, WI, 2001 version 6.12.
[20] Hydroxymethyldiphenylphosphine labelled with ^{13}C on the methylene carbon has been previously reported. Y. Kayaki, Y. Shimokawatoko, T. Ikariya, Inorg. Chem. 46 (2007) 5791–5797.
[21] [(a)] V. Maraval, R. Laurent, B. Donnadieu, A.-M. Caminade, J.-P. Majoral, Phosphorus, Sulfur, and Silicon 184 (2009) 1612–1620; [(b)] Y. Kayaki, Y. Shimokawatoko, T. Ikariya, Adv. Synth. Catal. 345 (2003) 175–179; [(c)] S. Gatard, S. Nlate, E. Cloutet, G. Bravic, J.-C. Blais, D. Astruc, Angew. Chem. Int. Ed. 42 (2003) 452–456.
[22] N. Feeder, J. Geng, P.G. Goh, B.F.G. Johnson, C.M. Martin, D.S. Shephard, W. Zhou, Angew. Chem. Int. Ed. 39 (2000) 1661–1664.

[23] [(a)] A.K. Pandiakumar, A.G. Samuelson, J. Chem. Sci. 127 (2015) 1329–1338; [(b)] I. Moldes, E. de la Encarnación, J. Ros, A. Alvarez-Larena, J.F. Piniella, J. Organomet. Chem. 566 (1998) 165–174.
[24] M. Esteban, A. Pequerul, D. Carmona, F.J. Lahoz, A. Martin, L. Oro, J. Organomet. Chem. 204 (1991) 421–434.
[25] [(a)] S.L. Apps, A.J.P. White, P.W. Miller, N.J. Long, Dalton Trans 47 (2018) 11386–11396; [(b)] Z.M. Heiden, S. Chen, M.T. Mock, W.G. Dougherty, W.S. Kassel, R. Rousseau, R.M. Bullock, Inorg. Chem. 52 (2013) 4026–4039.
[26] L.V. Graux, M. Giorgi, G. Buonoa, H. Clavier, Dalton Trans 45 (2016) 6491–6502.
[27] H. Werner, B. Klingert, A.L. Rheingold, Organometallics 7 (1988) 911–917.